WAVE EQUATION VELOCITY ANALYSIS

Alfonso González-Serrano and Jon F. Claerbout

Abstract

The retarded Snell midpoint coordinate frame enables us to interpret velocity analysis from the wave equation point of view. The imaging conditions applied to the coordinate transformation equations provide an exact way of estimating velocities in CMP gathers. Transforming the wave equation from physical variables to the new variables and putting the data into the new reference coordinates permits a migration, collapsing the energy toward the stationary part of skewed hyperboloids, where we can measure velocities as functions of event coordinates. Alternatively, we can project the data onto the t'-τ plane, where the energy will focus almost independently of the migration velocity and departures of the focused events from the expected coordinates give the true material velocities. This plane can be more appropriate for seafloor multiple removal. Both synthetic and real data examples of the first procedure are shown for the exact and 15-degree frequency-wavenumber domain operators.

Introduction

Seismic velocity determination is an iterative process. It may not seem to be iterative because the convergence can be so rapid that a satisfactory answer may be found after only one iteration. For example, in the industrial process called "brute stack" or "constant velocity stack," the assumption is made that the velocity is *constant*, thereby justifying the use of hyperbolic summation; thus, a *non-constant*, stratified velocity

is determined. Obviously, the ray paths are non-hyperbolic. So, in principle, further iterations of some kind should be done. In practice, it is not very clear how much we are missing if we fail to do so. We are unsatisfied with brute stack as a *definition* of velocity spectra and plan to seek a better definition.

Another problem in industrial velocity analysis is the matter that gates in time and midpoint are chosen somewhat arbitrarily. When we look at the low signal level seismic sections for weak events, we look at the section from various angles and at various distances, thereby selecting various gates. We need to try to display velocity information in seismic section form. It is not completely clear how this should be done, but we should probably avoid highly non-linear operations like semblance and keep the process linear on the data field. An article in SEP-15 ("Snell Waves," by Jon F. Claerbout, pp. 57-71) shows that it is possible for an observer to read interval velocity directly from the skewed CMP gathers, so non-linear methods like semblance are *not* necessary.

Still another objective of velocity analysis is to define stacking methods that not only emphasize some particular velocity but actually suppress other velocities. Consider the following "conventional" process, which we will call deH_20-1:

1) Stack at water velocity to get a good estimate of multiples.
2) Create a synthetic gather of multiples.
3) Subtract the synthetic multiples from the original data.
4) Stack at sediment velocity.

An alternative process could be defined with wave equations to achieve approximately the same objective. Call this deH_20-2:

1) Downward-continue to the focus predicted for water velocity.
2) Mute out zero offset and its vicinity.
3) Upward-continue at water velocity.
4) Downward-continue at sediment velocity.
5) Select zero offset.

How does the conventional process deal with angle dependence of reflection coefficient? Probably by automatic gain control. How does the wave equation deal with it? By definition of the size of the vicinity of the focus to be muted. This also takes care of the changes of wavelet with angles, which deH_20-1 can attack with time variable deconvolution. Factors that cause angle-dependent wavelets include elastic-propagation phenomena and shooting-recording arrays, to say nothing about lateral variations in the seafloor itself. The process deH_20-1 must somehow get these sorted out so that the subtraction in step (3) of the process works properly. The process deH_20-2 can bury most of such embarrassments by muting a larger zone about the water focus. It avoids the need for accurate multiple modeling.

Of course, neither of the deH_20 processes is very effective on peg-leg multiples, which are usually a more serious practical problem. What these simple processes are good for is to illustrate that it is time to have a good look at stacking and velocity spectra from a wave equation point of view. Not only that, but the history of migration via hyperbola summation versus migration via wave equation shows us that the wave equation methods have important advantages in that effects of aliasing, truncation, and resolving power can be explicitly analyzed and dealt with in a knowledgeable way. Wide angle problems that wave equation migration methods suffered in earlier years have been completely resolved by either the "phase shift method" or the "Muir recurrance method." Computational cost problems do not appear to be relevant in this age of array processors.

Advantages of retarded Snell midpoint coordinates

We are familiar with the idea that wave equation migration of horizontal beds is a rather trivial matter. As long as the output is taken to be a migrated time section instead of a migrated depth section, the output for a horizontal bed is completely correct, independent of an erroneous migration velocity. Turning our attention to a linearly moved out (LMO) common midpoint gather, we note that the flat part at the top of each skewed hyperboloid will not be moving as we upward- and downward-continue in a retarded Snell coordinate system. This means that this portion of the hyperbola is correctly upward- and downward-continued

despite any velocity errors. As we have seen in SEP-15 ("Snell Waves") the location of the skewed hyperboloid tops in fact gives us seismic velocity directly. The role of the migration velocity v(z) is to focus the energy at the tops. The advantages of the LMO may be summarized as: (1) velocity estimates are insensitive to *a priori* velocity information; and (2) for off-end recording, the LMO achieves a certain degree of spatial anti-aliasing.

There is not quite as much magic in the LMO as we first thought. A problem is this: although it is true that the hyperboloid top does not move, it is not true that the center of the energy of the focus does not move. This became quite evident in examples in which the energy distribution in the skewed hyperboloid was quite asymmetrical. The circumstance can be visualized if you were to have only one side from the top of the skewed hyperbola. (Examples are shown in the next section.) Best focus of the hyperboloid is still obtained at its top, but the center of energy moves laterally in some rough proportion to the average dip, the downward-continuation velocity, and the depth. So the center of energy of a focus is not so independent of the a priori velocity as is the hyperboloid top. As a result of this, we have come to view velocity analysis as a study not just in the offset-time (h,t') plane, as suggested in SEP-15 ("Short Review of Retarded Snell Midpoint Coordinates," by Jon F. Claerbout, pp. 81-87), or in the time-depth (t',z) plane, as suggested in SEP-1 (Doherty and Claerbout, pp. 160-178), but as some analysis in the (h,t',z) volume. Since we cannot make a satisfactory display of the volume, our next plan is to display a surface in (t',z) [or (t',τ) where τ is a "migration depth"] for that value of h which is determined for the *a priori* migration velocity.

Theory

The transformation from physical variables (shot-geophone) to the retarded Snell midpoint coordinates is given by (Claerbout, SEP-15, p. 81):

$$t' = t - p(g - s) + 2\int_0^z \frac{\cos\,\theta}{v}\,dz \qquad (1a)$$

$$y = \frac{g + s}{2} \tag{1b}$$

$$h = \frac{g - s}{2} + \int_0^z \tan\theta \, dz \tag{1c}$$

$$\tau = 2\int_0^z \frac{\cos\theta}{v} \, dz \tag{1d}$$

where (s,g,z,t) = (shot,geophone,depth,time) are the recording coordinates, and (h,y,τ,t') = (half offset,midpoint,traveltime depth, retarded time) are the new reference coordinates.

Substituting the imaging conditions $s = g$, $t' = \tau$ yields an exact expression for the interval velocity estimation (Claerbout and Lynn, SEP-14, pp. 73-80):

$$v^2 = \frac{1}{p\left(p + \frac{1}{2}\frac{dt'}{dh}\right)} \tag{2}$$

It can be particularly useful to downward-continue the data to enhance the signal-to-noise ratio, and consequently improve the velocity estimation. This is easily achieved in the frequency-wavenumber (f-k) domain: call $P(k_h,\tau=0,\omega)$ the data transformed into f-k space, then use a modified dispersion relation for the telescope equation:

$$P(k_h,\tau,\omega) = P(k_h,\tau=0,\omega)\, e^{i\int_0^\tau k_\tau d\tau} \tag{3}$$

where k_τ is given by

$$\frac{k_\tau}{\omega} = 1 - \frac{pv}{1 - p^2v^2} H - \sqrt{1 - \frac{2pvH + H^2}{1 - p^2v^2}} \tag{4}$$

$$H = \frac{k_h v}{2\omega} \tag{5}$$

Next we substitute the imaging conditions $t' = \tau$, to get the migrated time gather:

$$P(h,\tau,t'=\tau) = \iint_{-\infty}^{\infty} P(k_h,\tau=0,\omega)\ e^{i\int_0^{\tau}(k_\tau-\omega)d\tau}\ e^{ik_h h}\ dk_h\ d\omega \tag{6}$$

The 15-degree approximation is found by expanding the square root from Equation (4) and retaining the terms up to the second degree in H, giving

$$\frac{k_\tau}{\omega} = \frac{H^2}{2(1 - p^2v^2)^2} \tag{7}$$

For time domain computations, this equation takes the form,

$$P_{\tau t'} = -\frac{v^2}{8(1 - p^2v^2)^2} P_{hh} \tag{8}$$

If we look for a projection of the data in the t'-τ plane rather than the usual h-τ plane, then we need to decide which value of h to display using Equations (1a) and (1c). Substituting the stopping condition $s = g$, we get the new condition,

$$\bar{h} = \frac{1}{2}\int_0^{t'} \frac{pv^2}{1 - p^2v^2}\, dt' \tag{9}$$

Using this equation we get from Equation (3):

$$P(h=\bar{h},\tau,t') = \iint_{-\infty}^{\infty} P(k_h,\tau=0,\omega)\; e^{i\int_0^{\tau} k_\tau\, d\tau}\; e^{ik_h\bar{h} - i\omega t'}\; dk_h\, d\omega \qquad (10)$$

This new plane will have the events aligned along the 45-degree slope, if the migration velocity is correct, and will focus the events somewhere else depending on their velocity.

To get a relationship to estimate velocity, we can use Equation (2). Remember that all events displayed for a given τ have a common offset; then we can substitute for both the downward continuation velocity (v_m) and the true velocity (v_e). After eliminating h and solving for v_e, we get

$$v_e^2 = \frac{1}{\frac{dt'}{d\tau}\left(\frac{1}{v_m^2} - p^2\right) + p^2} \qquad (11)$$

Examples

Figures 1, 2 and 3 show synthetic examples for the (h,t') and (h,τ) planes computed in the frequency-wavenumber domain. Figure 4 is the field data gather for the test with real data: the results are shown in Figures 5-10. Figures 5 and 6 show the data resampled at 0.008 sec with an LMO correction applied. These figures also display the reference grid for velocity estimations. Figures 7-10 show the migrated results for the exact and 15-degree approximation operators

for two different values of p. The data of these figures was low-pass filtered to remove high frequency noise. Details are on the figure captions.

Figure 11 shows a synthetic gather without seafloor multiples as an example of the first three steps of the deH_20-2 procedure. Finally, Figures 12 to 15 show examples in the (t',τ)-plane for $p=0$.

ACKNOWLEDGMENT

The first author would like to thank S. M. Deregowski for his suggestions during the programming stage of this project. The data used was from Amoco Flemish Cap, East Coast of Canada.

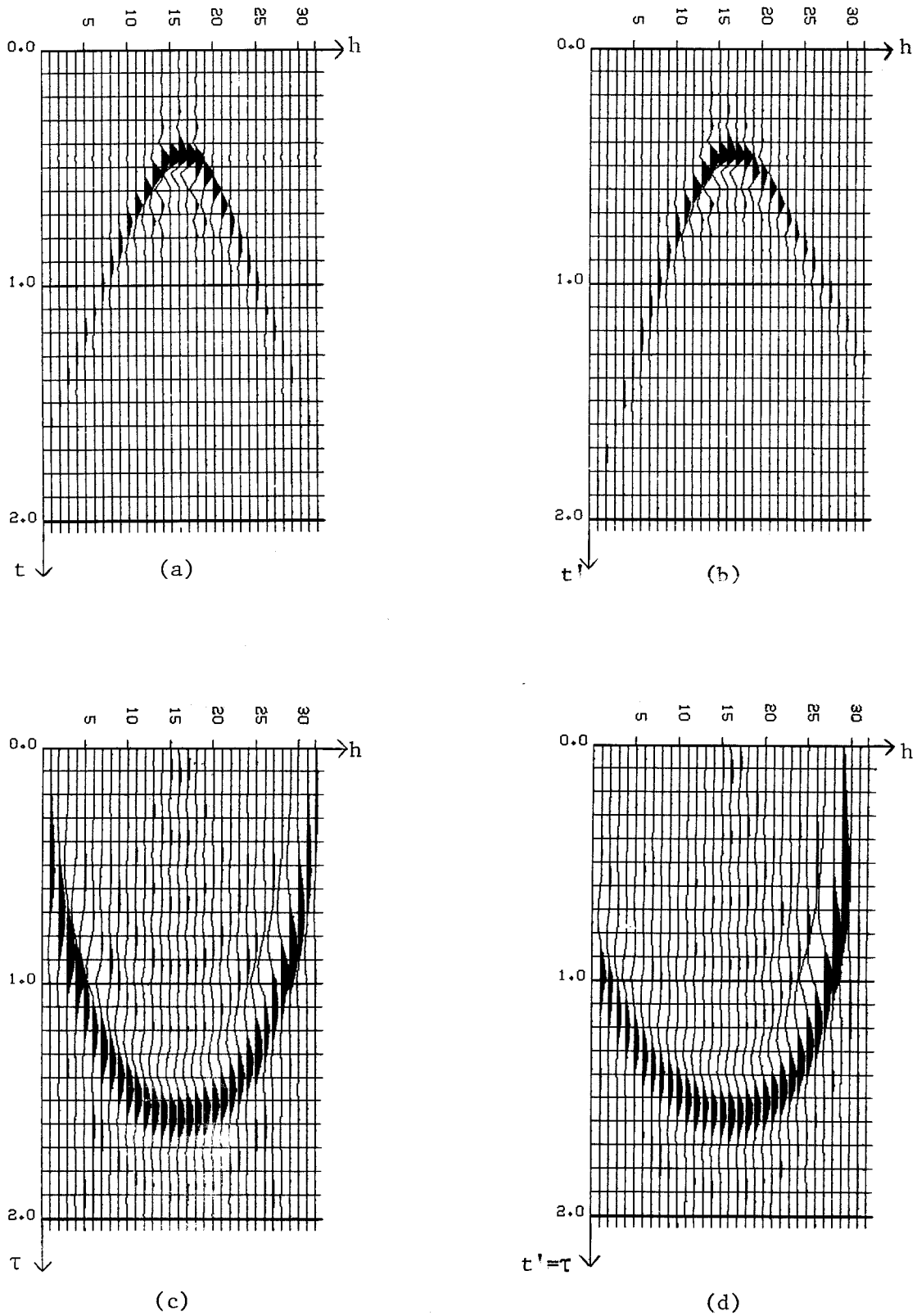

FIGURE 1.--Impulse response for the diffraction and migration transfer functions: (a) is the conventional diffraction with $p = 0$, while (b) has a ray parameter $p = 1/5000$ sec/m, thus getting a skewed hyperbola; (c) and (d) are the impulse response of the downward-continuation operator.

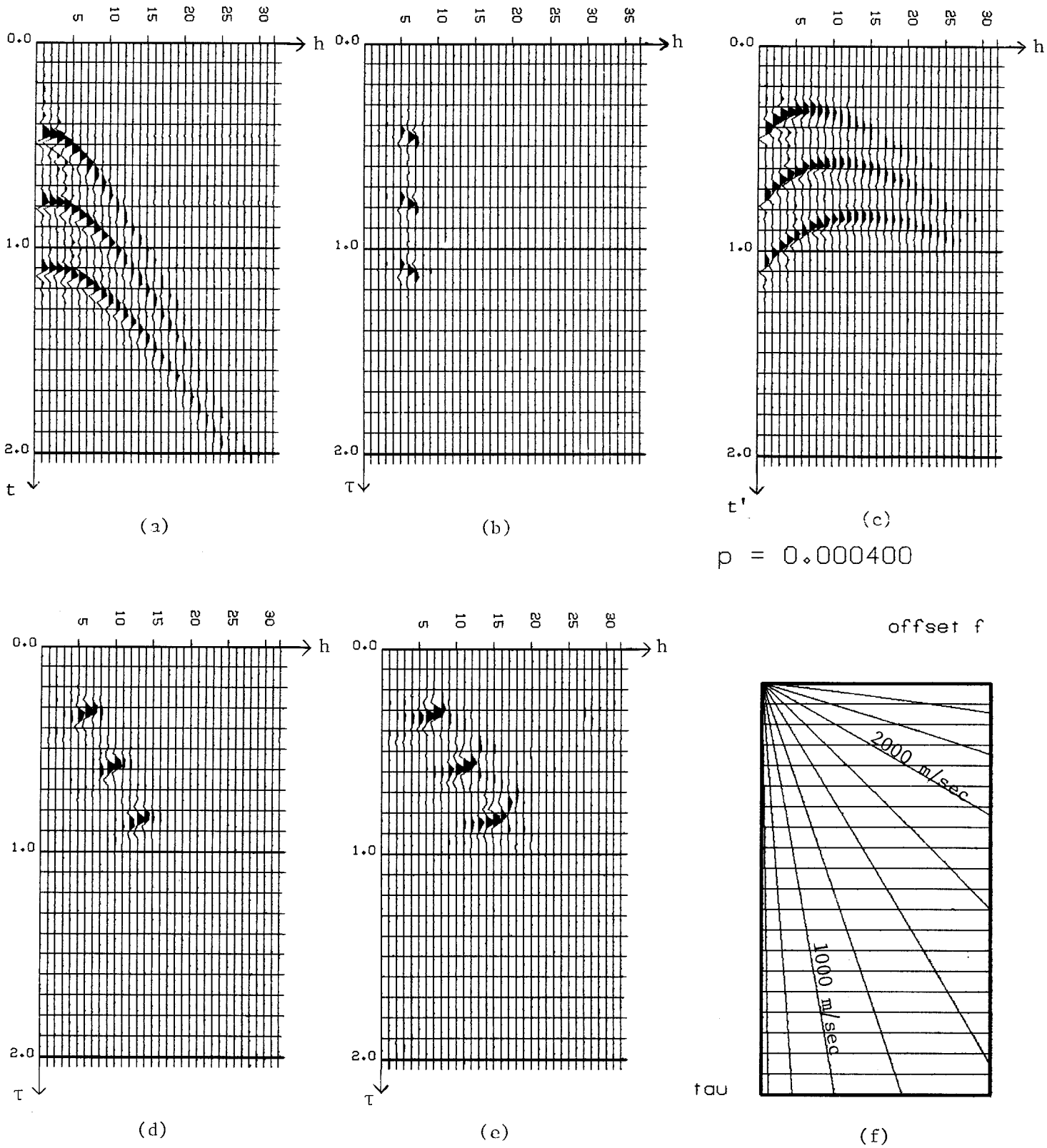

FIGURE 2.--Constant velocity example: (a) is the diffracted data for a velocity of 1500 m/sec; (b) is the conventional collapse using the wave equation in (h,t)-coordinates. (c) is the LMO-corrected gather with a value of p = 1/2500 sec/m. (d) is the exact equation result, while (e) is the downward-continuation using the 15-degree equation. We see the 15-degree equation gave reasonable results, with minor trouble due to the steep slope to the left of the tops of the hyperboloids in the gather. With the aid of (f), we can measure the interval velocities directly comparing the slopes between events in the migrated gathers.

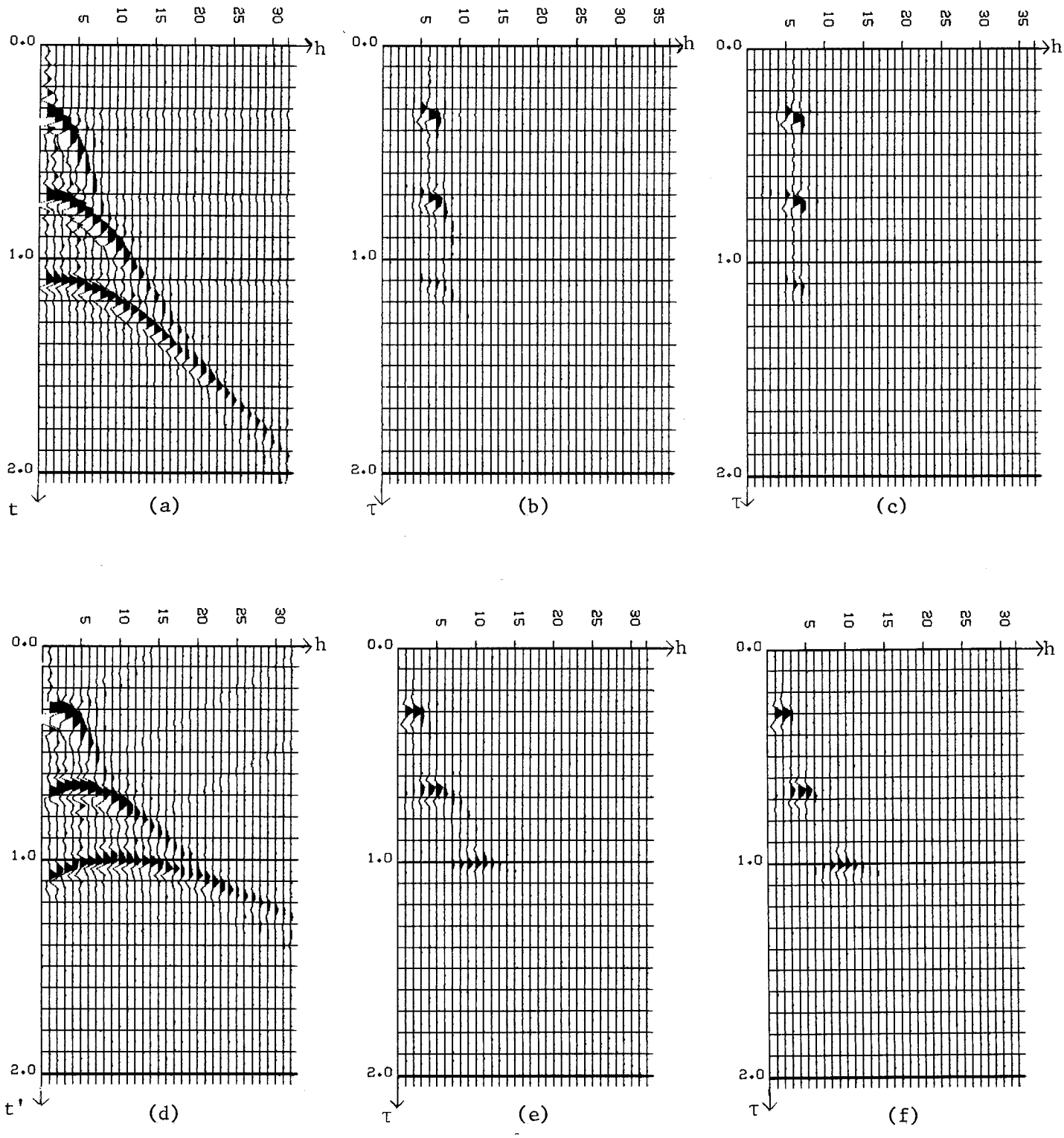

FIGURE 3.--Variable velocity case: (a) is the synthetic gather; (b) is a 15-degree migration; and (c) is an exact migration for $p = 0$. The first event has a wider range of spatial k_h frequencies, giving a sharper focus with respect to the other two. (d) has an LMO-correction, using $p = 1/5000$ sec/m. (e) and (f) are the migrations using the correct velocities for the 15-degree and exact equations respectively. The energy in the lower right part of (e) corresponds to the very steep slope of the first hyperbola, and the tail at the right of the second focused event is energy that was not correctly handled by the 15-degree equation but presenting no problem to the exact equation. For the third event, the LMO-correction has reduced the steep slopes, so we get a better though (cont.)

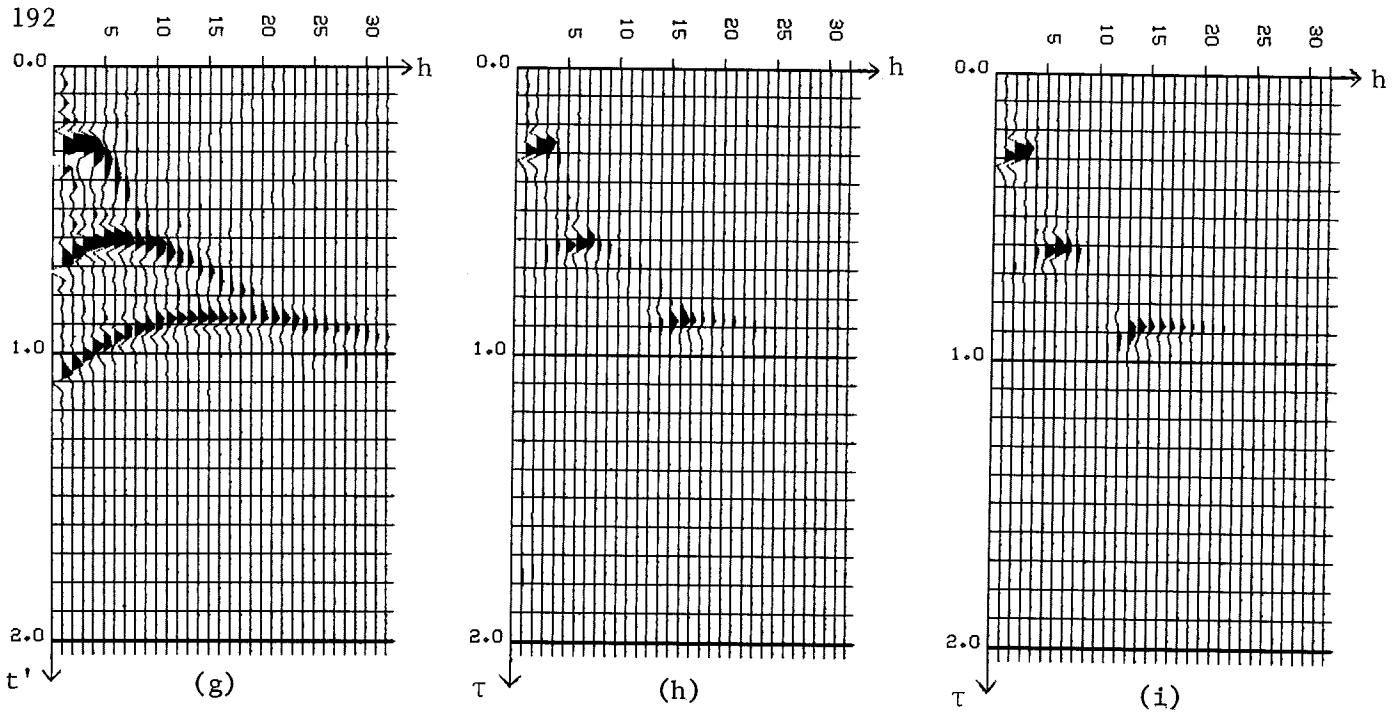

p = 0.000200

p = 0.000300

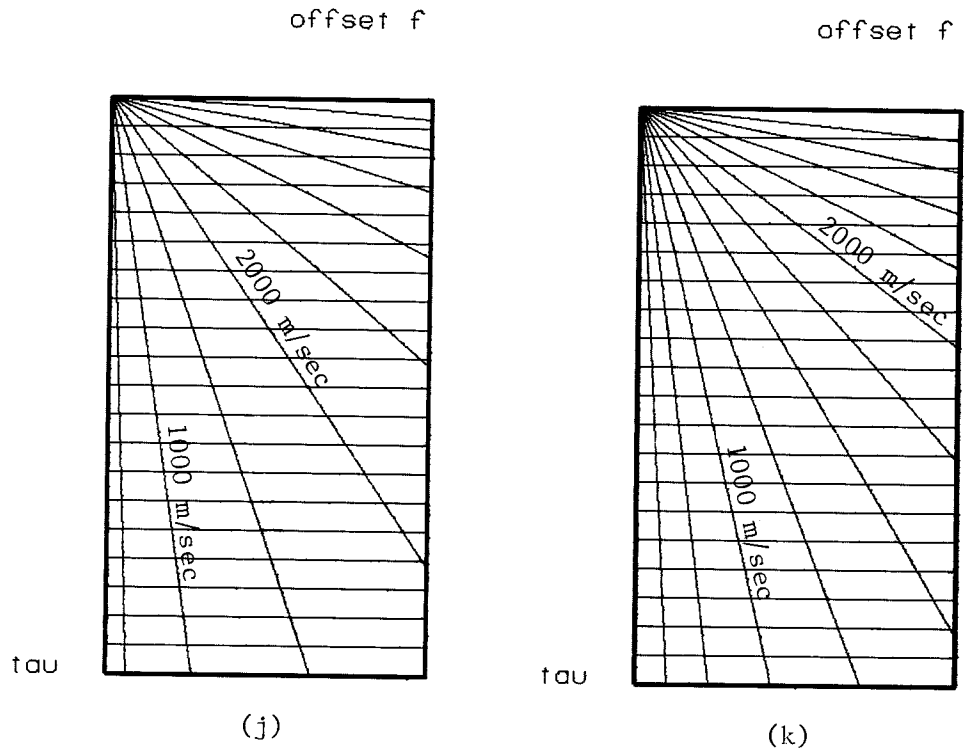

(Figure 3 cont.) broadened focus because of this reduction. (g,h,i) are similar to (d,e,f) respectively, but for a value p = 1/3333 sec/m. Here the 15-degree equation handled the third hyperbola remarkably well, while the exact operator had trouble with the now wider flat part of the skewed hyperboloid where the exact operator is null. (j) and (k) are the reference grids for velocity estimation.

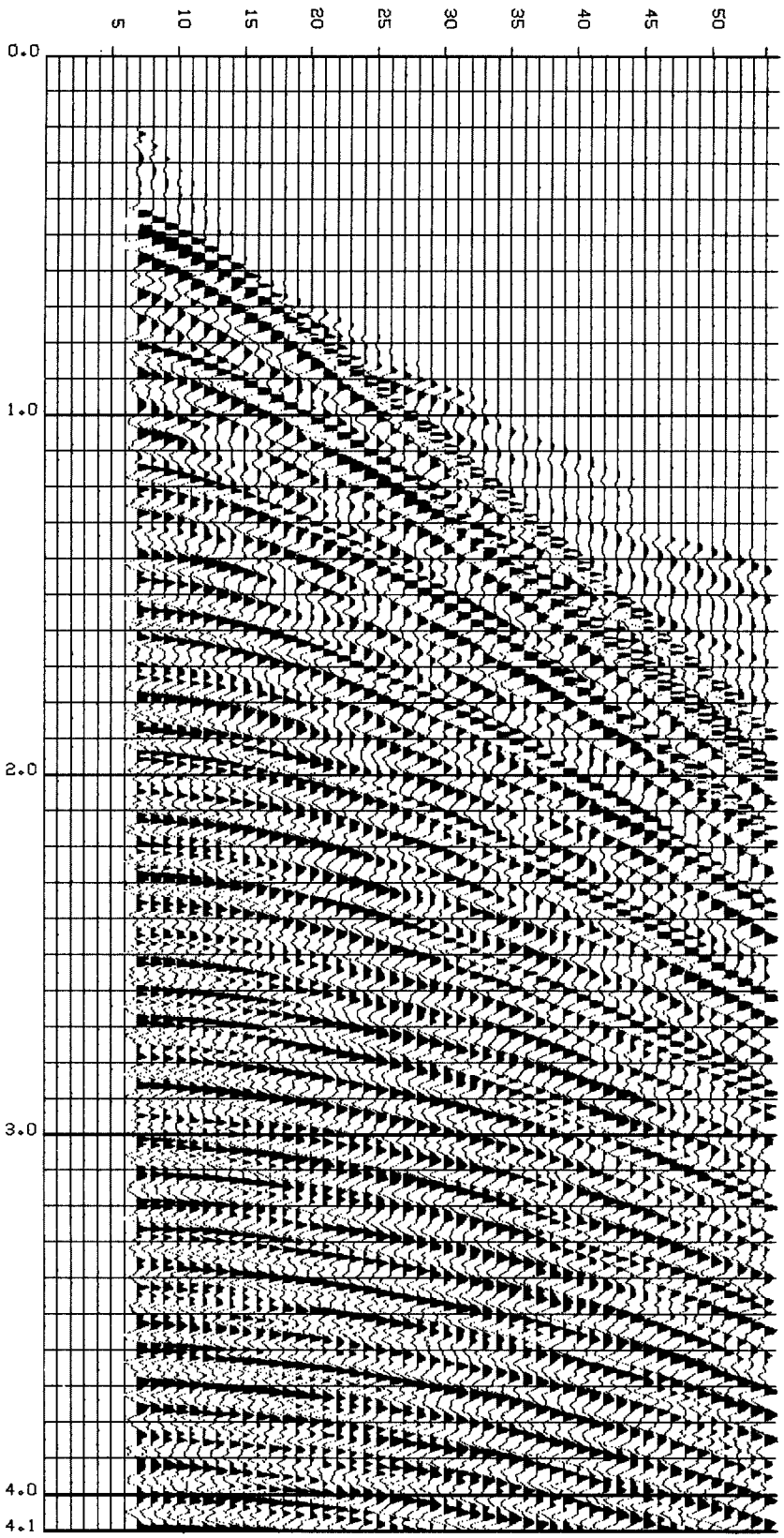

FIGURE 4.--Common midpoint gather for field data examples. The data is a 48-trace gather sampled at 0.004 sec. The trace separation is 50 m with in-line offset of 273 m.

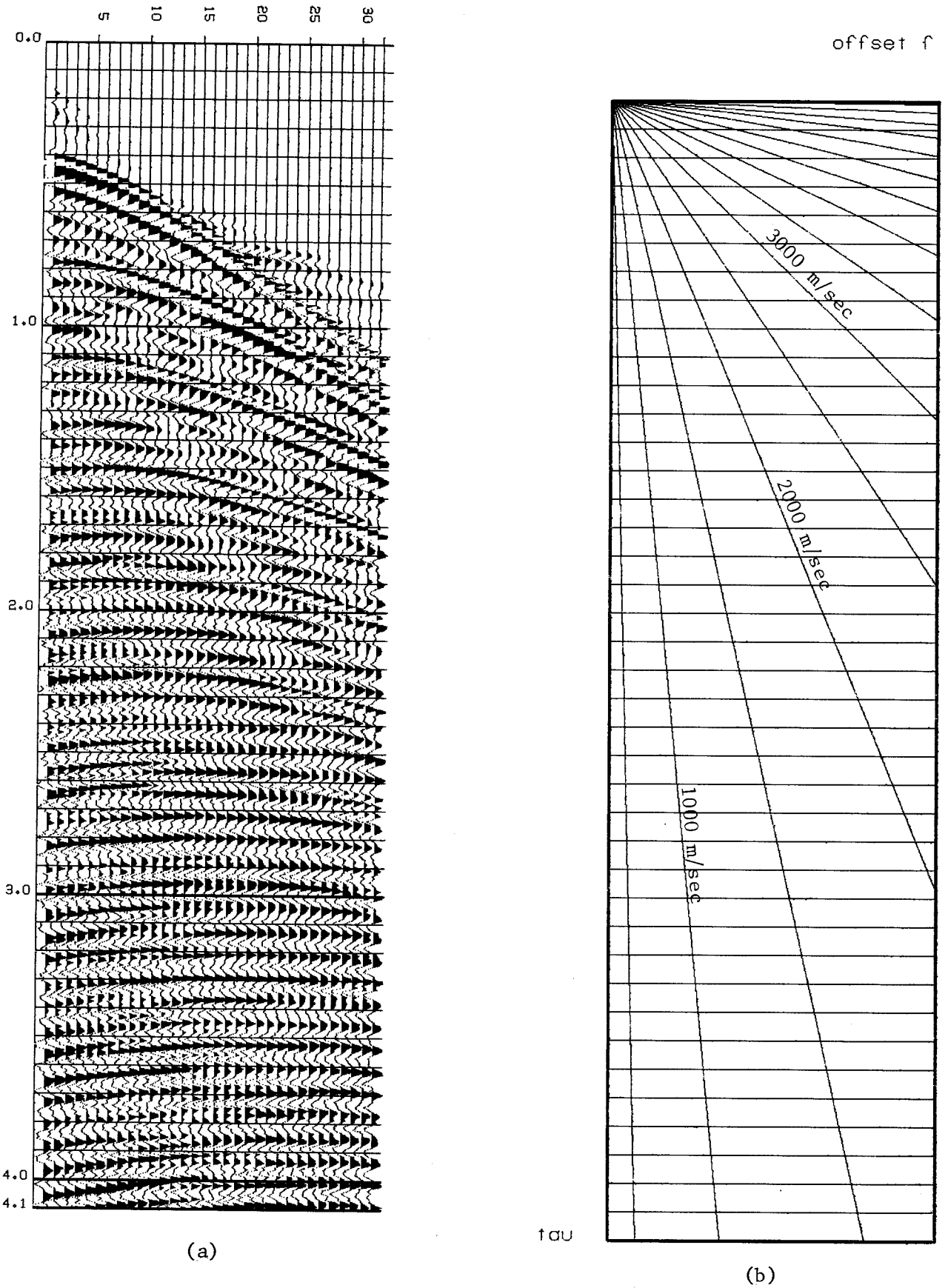

FIGURE 5.--Data with LMO-correction using p = 1/7700 sec/m. The data was resampled to 0.008 sec, and only the first 32 near traces were used. (b) shows a reference grid for interval velocity determination.

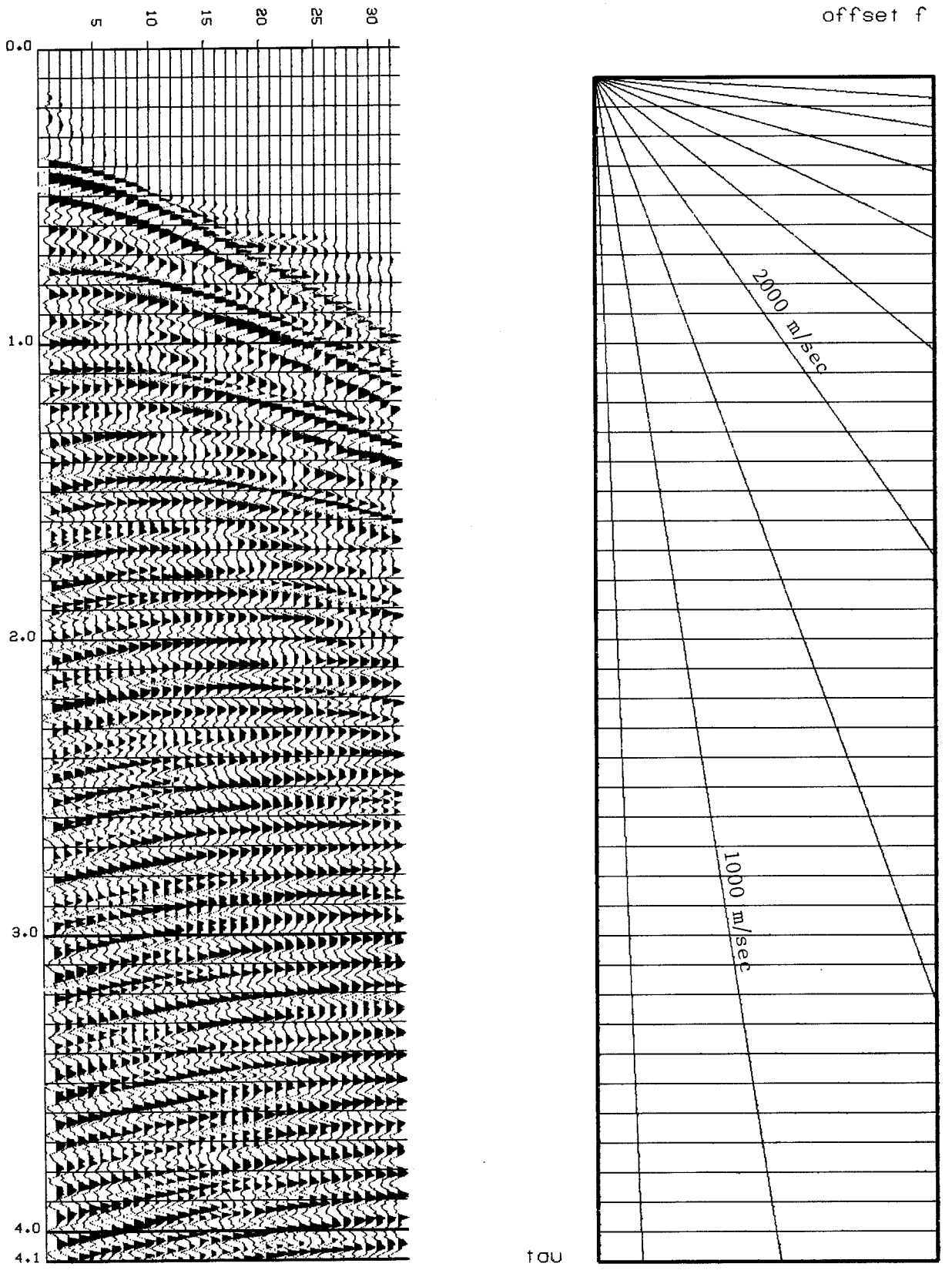

(a) (b)

FIGURE 6.--Data with LMO-correction using p = 1/5000 sec/m.

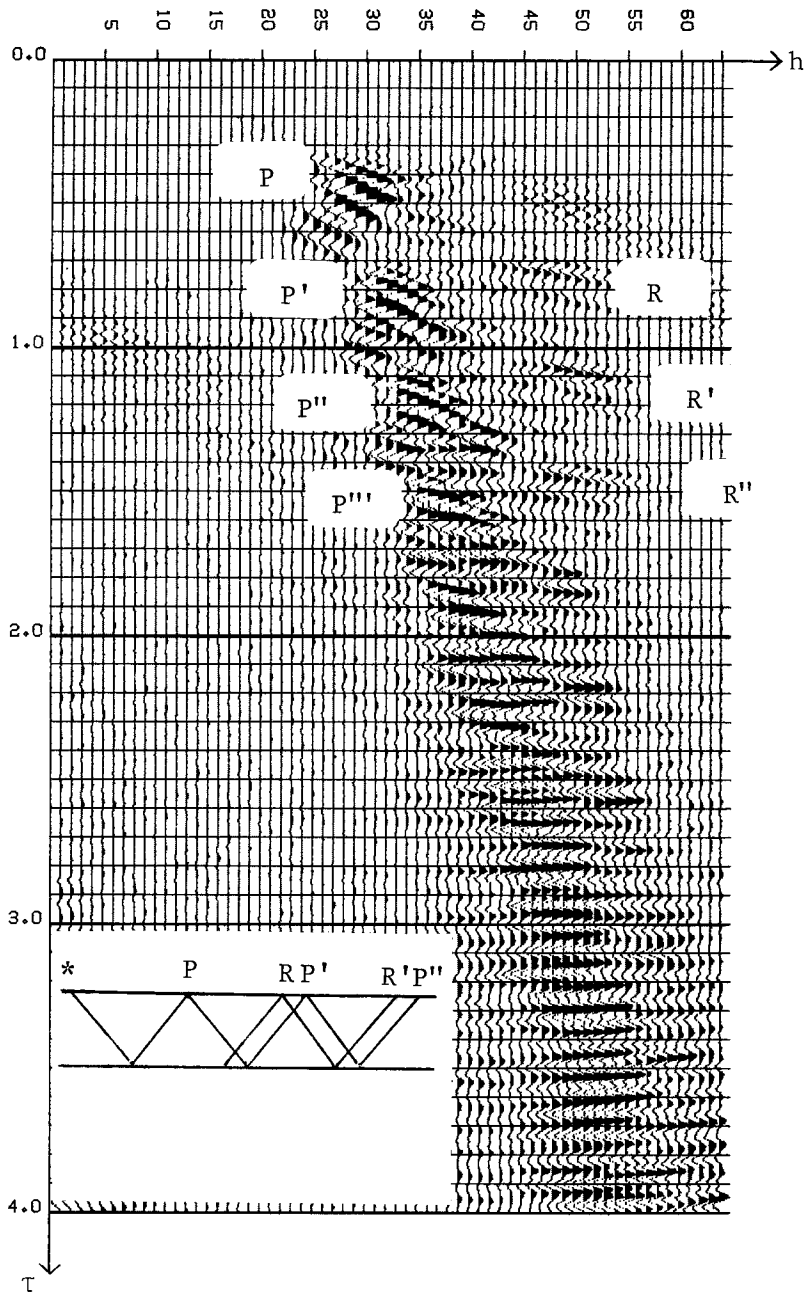

FIGURE 7.--Migration with 90-degree equation for the data of Figure 5. The migration velocity is 1450 sec/m with p = 1/7700 sec/m. The zero-offset trace corresponds to the trace number 27 approximately, and the first trace of the gather starts at trace number 33. The 64 traces are displayed to show the effect of wrap-around. The gather was padded with zeros to double its size before migration. We can easily identify all the seafloor multiples aligned along the water velocity line, also the multiple refractions from the event at 0.75 (trace 49) can be followed with its associated phase reversals clearly visible; another refraction at 0.55 sec (trace 37) can be followed with its corresponding multiples. The high frequency noise between traces 40-64 (0.62 to 0.95 sec) is associated with the seafloor reflection. Note also that the tops of the hyperboloids are in the expected positions; however, the energy is not concentrated at the top due to the asymmetry of the input data and migration process. This can introduce a biasing effect in the velocity estimates. Also note that it is not easy to recognize events for velocities not close to the migration velocity, while a stratified velocity migration will not separate the seafloor multiples so nicely. This makes it attractive to work instead in the (t',τ)-space.

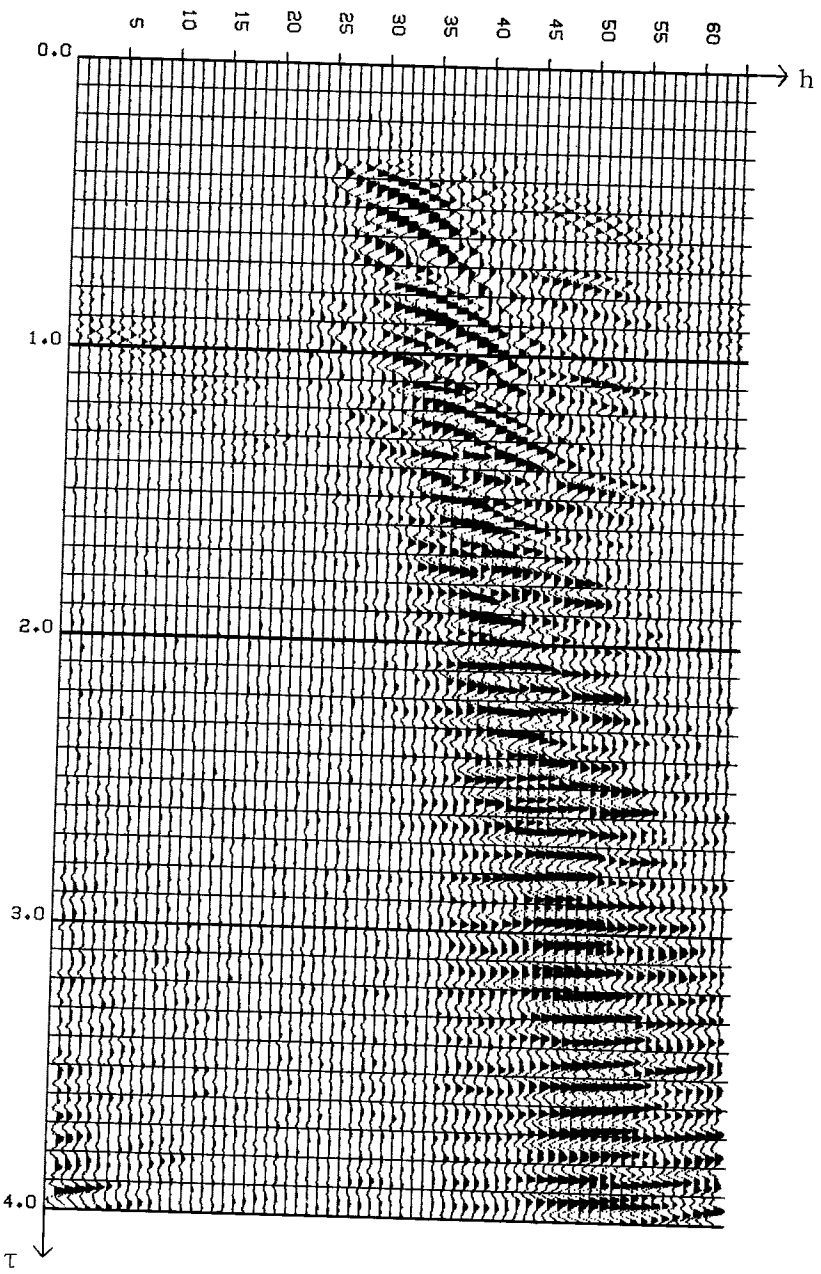

FIGURE 8.--Same as Figure 7 for the 15-degree equation. We have now wider asymmetrical focus associated with the seafloor multiples because of the restricted range of spatial frequencies.

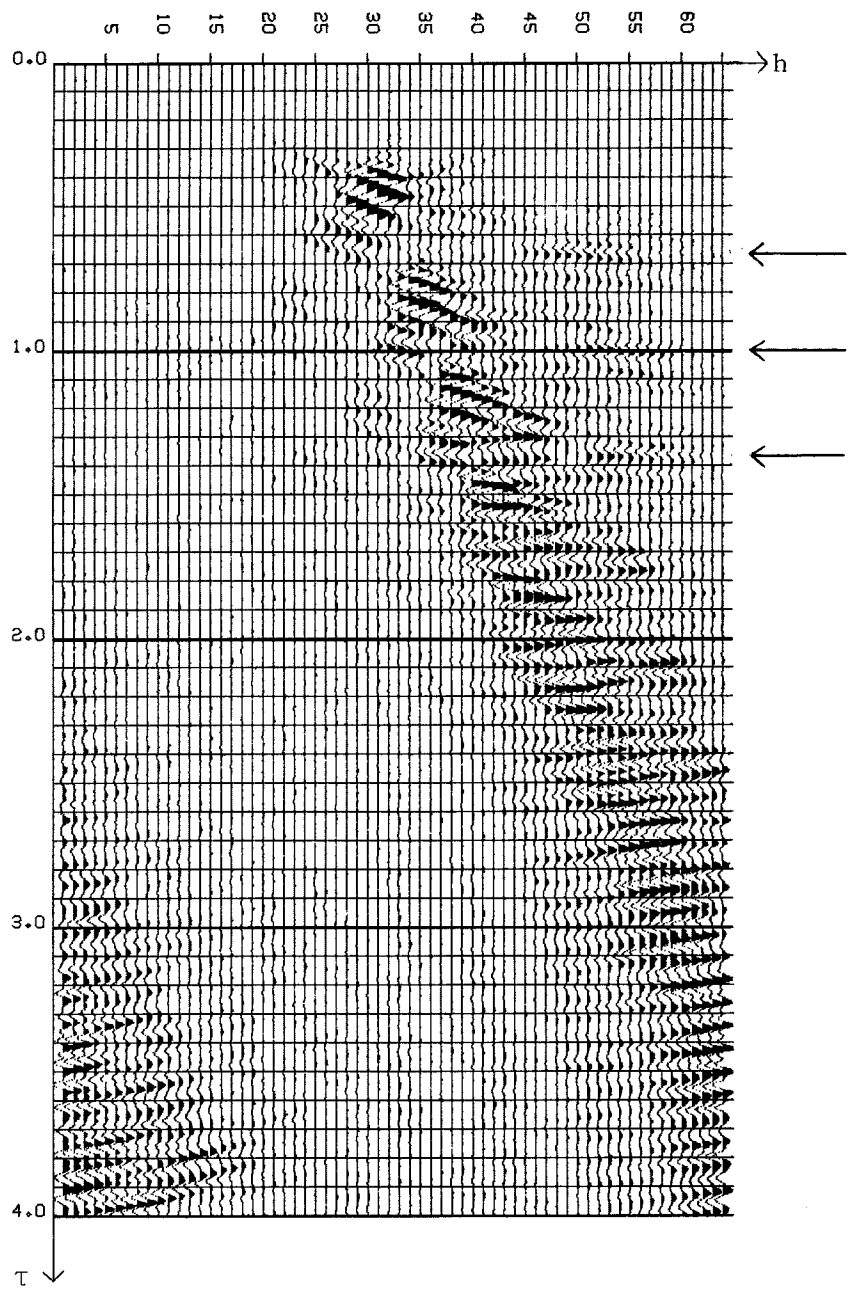

FIGURE 9.--Migration with 90-degree equation for the data of Figure 6. The migration velocity again is v = 1450 m/sec, but for a p = 1/5000 sec/m. We recognize the same characteristics as in Figure 7; however, this value of p makes multiple refractions more visible. Note the change in polarity of the multiples and peglegs.

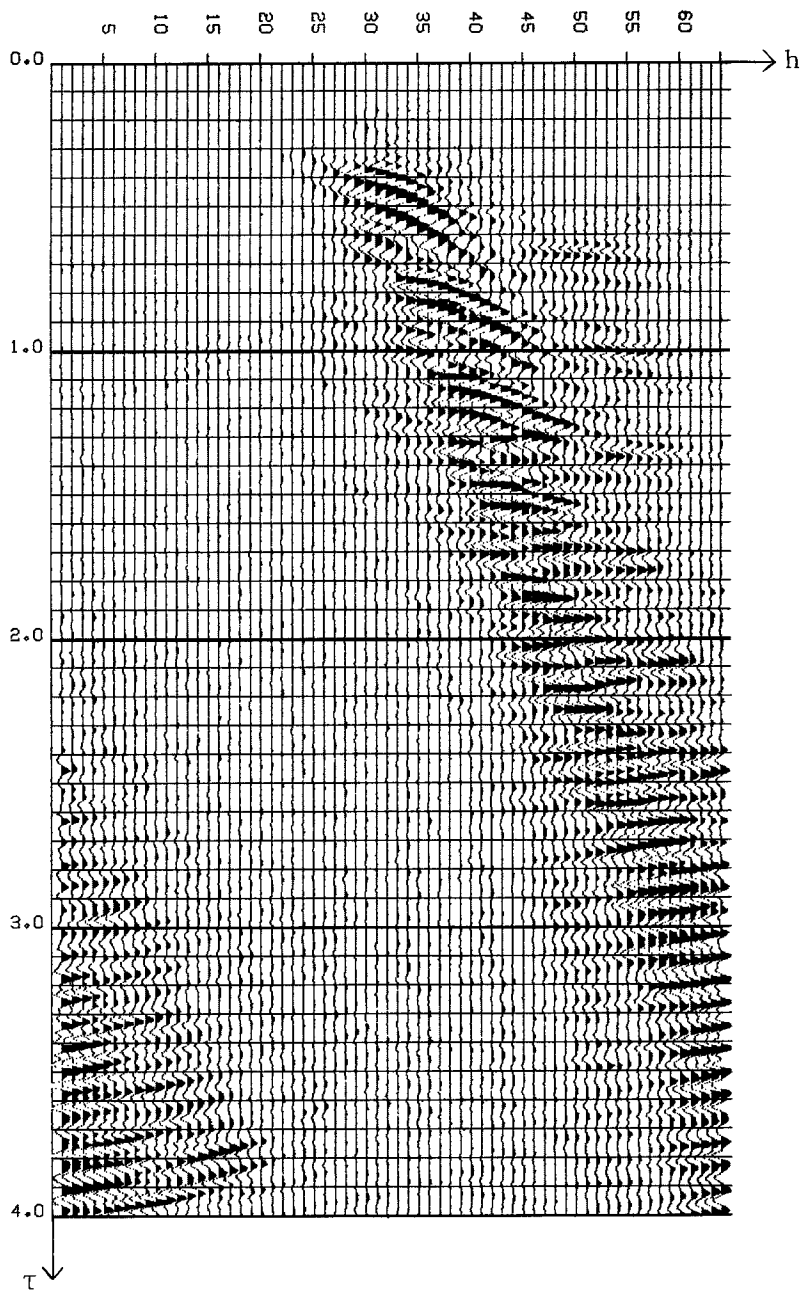

FIGURE 10.--Same as Figure 9 for the 15-degree equation.

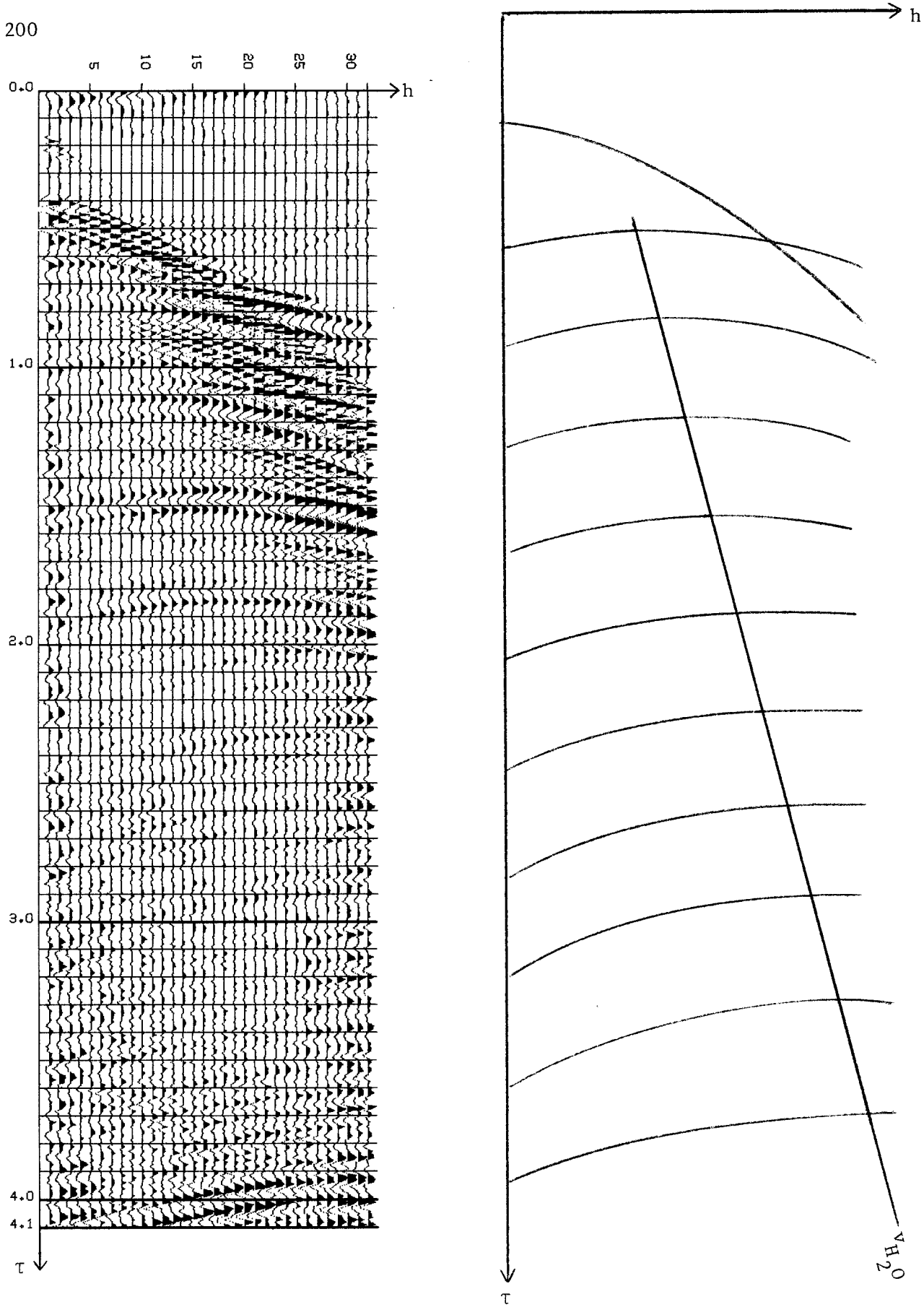

FIGURE 11.--Synthetic gather from the data of Figure 7. This figure was obtained by muting along the 2000 m/sec velocity line in Figure 7 and upward-continuing the data. As expected, we have suppressed a great part of the seafloor multiple energy so the peglegs associated with the refractions are much more visible than from the original data in Figure 5. (p = 1/7700 sec/m).

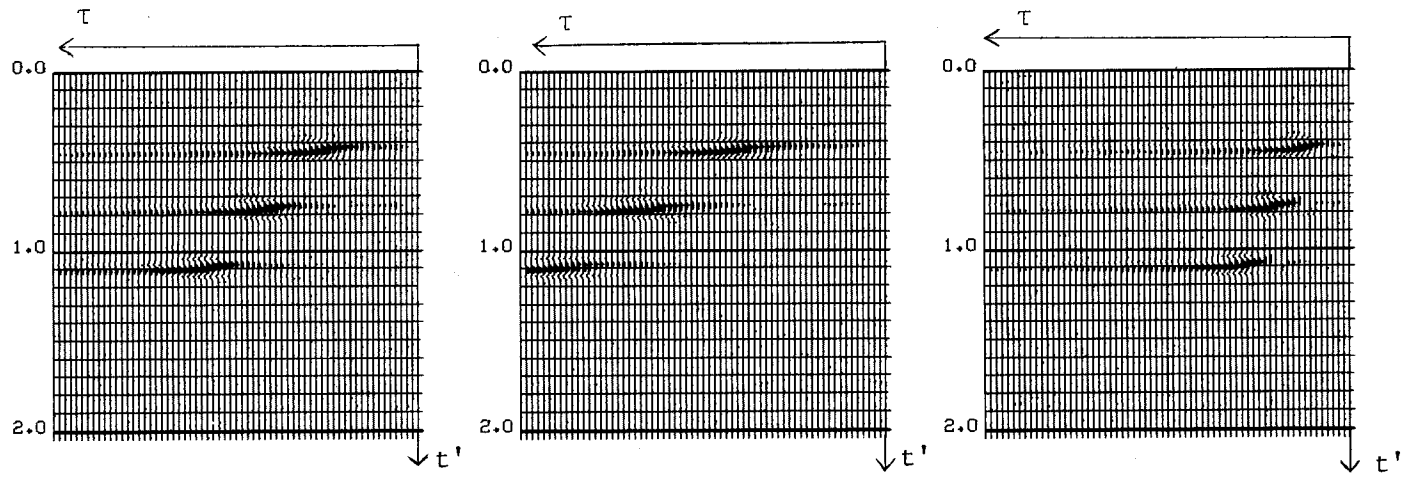

(a) (b) (c)

FIGURE 12.--Constant velocity example illustrating the results of displaying the (t',τ)-plane. The input data is from Figure 3a. (a) shows the result using the exact velocity (1500 m/sec), with the events aligned along the $t'=\tau$ line; note the 90-degree phase shift associated with the two-dimensional focusing as mentioned in SEP-1. (b) was downward-continued for v = 1250 m/sec; now that the events are above the t' = slope, we can use Equation (11) to find the material velocity from the new slope of the events. (c) is an example using a faster velocity v = 2000 m/sec, thus getting the events aligned below the $t'=\tau$ line.

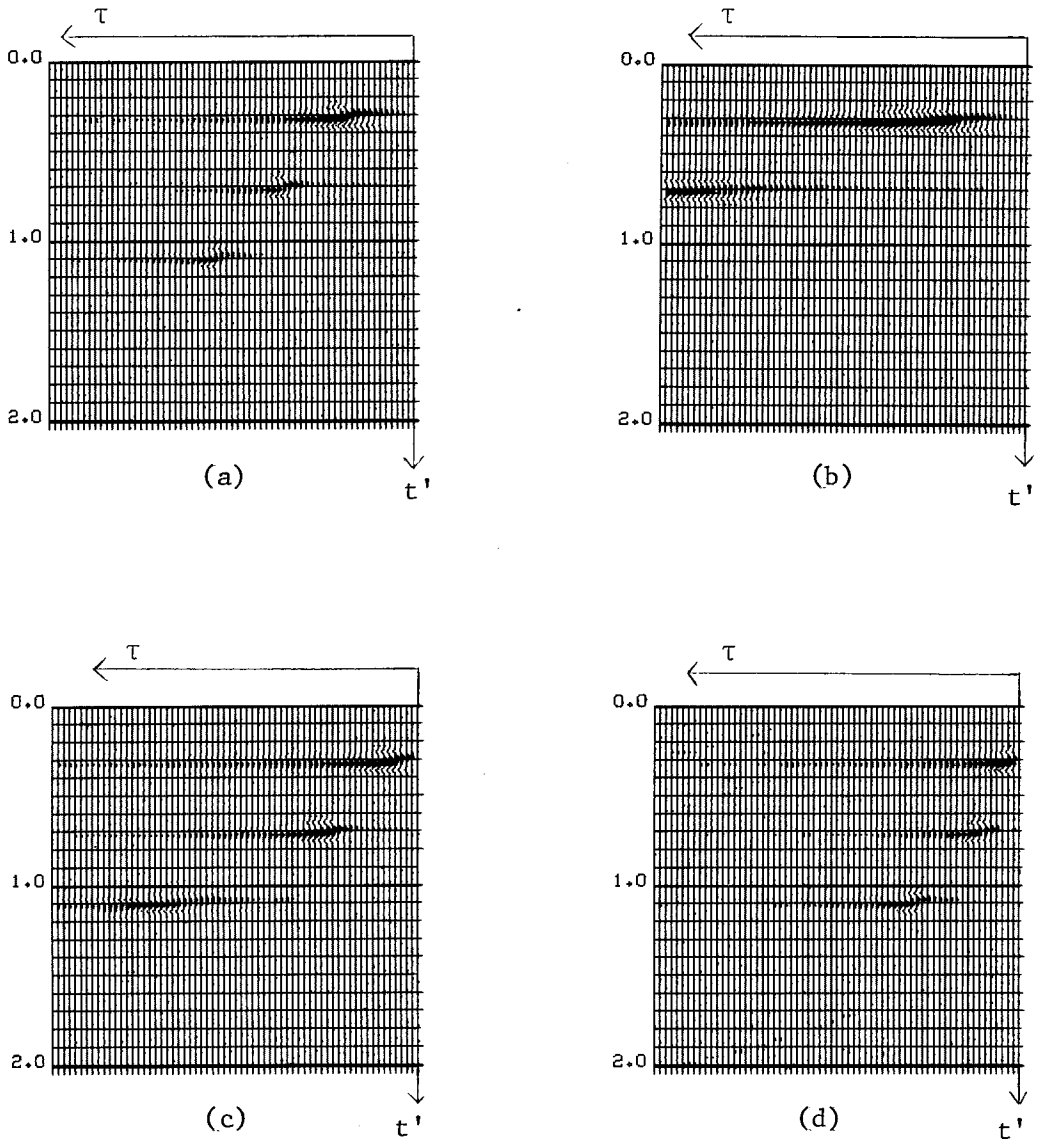

FIGURE 13.--Variable velocity example. The input data is from Figure 4(a). (a) is the exact result using the correct velocities, with the events aligned along the $t'=\tau$ line. (b) is the result using the velocity for the first event, so its focus has the expected 45-degree slope, while the other two events with higher velocity have smaller slopes. Note the downward-continuation steps were insufficient to at all focus the third event. In (c) we used the velocity for the second event; note that the slope between the origin and the first event is greater than 45 degrees. (d) was downward-continued using the velocity for the third event, so now the slope between the second and third events is 45 degrees exactly. This figure emphasizes the fact that in the (t',τ)-plane we get focusing of the events independently of the downward-continuation velocity, and departures from the expected coordinates give the information necessary to find the correct velocity. Also note that if we measure the slopes with respect to the origin to an event we get the RMS velocity for that event, and if we measure the velocity between two events, we get the RMS velocity between those events.

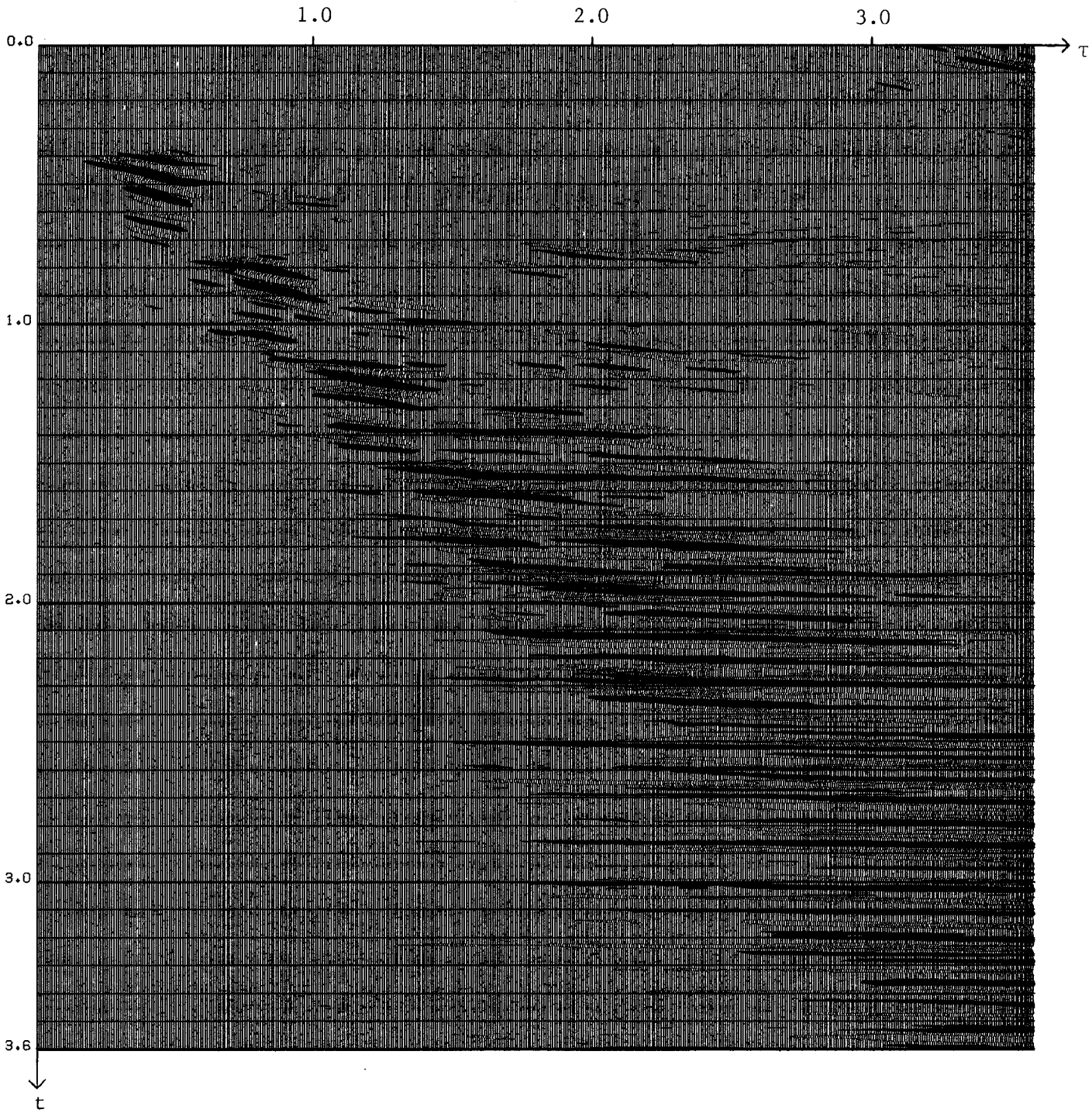

FIGURE 14.--This figure shows the downward-continuation of the data in Figure 4, displaying the zero-offset traces at each step. The velocity for the downward-continuation was 1450 m/sec. We expect the sea bottom primary and its multiples to be aligned along the $t=\tau$ line. The energy of the upper right corner is due to the effects of wraparound and cable truncation. The event at $t = 0.55$ sec, $\tau = 1.0$ sec is the sea bottom refraction; its associated peglegs can be distinguished aligned with a 45-degree slope below this event.

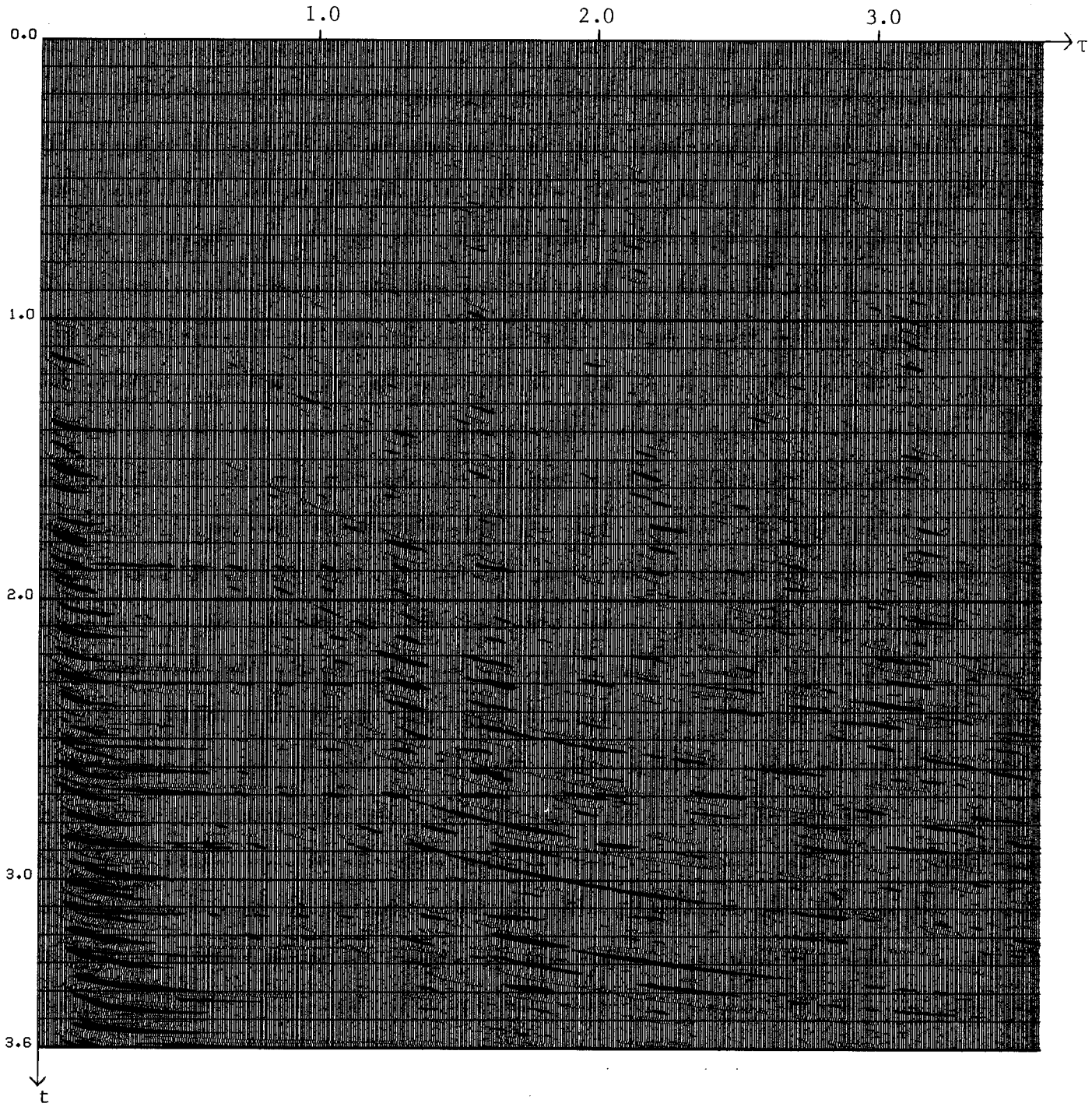

FIGURE 15.--This figure shows the downward-continuation of the data in Figure 4, again displaying the zero-offset trace at each step and using a downward-continuation velocity of 5500 m/sec. Now the sea bottom primary and its associated multiples come to focus very early. For shallow events the downward-continuation steps were too long to get a good focusing. For this high velocity, the effects of wraparound and cable truncation are very severe or can be seen from all the diffracted energy in the grid.